KINEMATIC ANALYSIS OF A TRANSLATIONAL 3-DOF TENSEGRITY MECHANISM

Chris Mohr[1], Marc Arsenault[2]

[1] *Department of Mechanical and Aerospace Engineering, Royal Military College of Canada, chris.mohr@rmc.ca*

[2] *Department of Mechanical and Aerospace Engineering, Royal Military College of Canada, marc.arsenault@rmc.ca*

Abstract

This paper presents a novel three-degree-of-freedom mechanism based on a known tensegrity architecture. The mechanism is cable driven and shown to exhibit three-dimensional translational motion. Analytical solutions to the direct and inverse kinematic problems are produced based on the geometry and statics of the mechanism. The boundaries of the Cartesian workspace are developed based on maintaining valid tensegrity configurations and requiring the actuated cables to be in tension. The low inertia, relatively large workspace volume and the movement produced by the mechanism make it promising for high speed applications such as pick and place operations.

Keywords: tensegrity, kinematic analysis, workspace.

ANALYSE CINÉMATIQUE D'UN MÉCANISME DE TENSÉGRITÉ AVEC TROIS DEGRÉS DE LIBERTÉ EN TRANSLATION

Résumé

Cet article introduit un nouveau mécanisme à trois degrés de liberté qui est développé à partir d'une architecture de tenségrité connue. Le mécanisme est entraîné par câbles et sa plate-forme mobile se déplace en translation. Des solutions analytiques aux problèmes géométriques direct et inverse du mécanisme sont développées à partir de sa géométrie et de son équilibre statique. Les frontières de l'espace atteignable du mécanisme sont calculées à partir de la nécessité de ce dernier de demeurer dans des configurations de tenségrité tout en soumettant ses câbles à des forces en tension. L'inertie réduite des parties mobiles du mécanisme ainsi que son espace atteignable relativement grand et son mouvement en translation en font un candidat intéressant pour les applications nécessitant des mouvements rapides comme, par exemple, les opérations de transfert.

Mots-clé: tenségrité, analyse cinématique, espace atteignable.

1 INTRODUCTION

The demand for robots in industry is constantly increasing and, in many applications, it is desirable for these robots to move as quickly as possible. However, there are physical limitations on the maximum speed of manipulators due to the forces required to accelerate their linkages. There are two main approaches to addressing this issue: either stronger, and usually larger, actuators must be used, or the mass of the linkages must be reduced. Parallel mechanisms achieve the latter by utilizing lightweight, rigid arms and typically locating actuators at their stationary base. Tensegrity mechanisms could further reduce their inertia, and thereby further increase their maximum speed, by their extensive use of low mass cables rather than solid links.

Tensegrity is a compound of the words 'tensile' and 'integrity'. Although he did not solely discover the concept, American architect Buckminster Fuller [1] first coined the word tensegrity to describe a structure composed of axially loaded compression members held together within a network of tension cables. By loading these elements appropriately, static equilibrium can be achieved and the structure experiences a state of self stress, requiring no external forces to remain rigid. The lengths of individual elements within tensegrity structures can be strategically actuated. Variations in these lengths can be controlled to cause desirable changes to the structures' geometry, leading to their possible use as robots.

Several applications of tensegrity-based mechanisms already exist. These applications range from deployable satellite antennae [2] to flight simulators [3]. There have also been several proposed designs for mobile robots that use tensegrity mechanisms to produce gait [4] and snake-like locomotion [5]. Additionally, due to their architecture and behaviour, tensegrity mechanisms have lent themselves well to being used as both planar and spatial robotic manipulators [6, 7].

Tensegrity mechanisms have many potential benefits. Elements within a tensegrity remain axially loaded at all times and do not experience bending moments. This allows thinner and lighter members to be used without adversely affecting the strength of the structure as a whole. Additionally, there is the possibility of simple deployment since manipulating tension within members can allow the entire structure to erect or collapse itself, as shown by Sultan and Skelton [8] and Duffy *et al.* [9]. As already mentioned, the elements of a tensegrity mechanism can be extremely light and incorporate cables that can be driven by stationary actuators, as shown by Mirats-Tur [10]. This greatly reduces the mass of moving parts, and therefore inertia, potentially allowing for higher accelerations. Finally, tensegrity mechanisms incorporating cables generally do not require the complete surrounding of their end-effector by wires to be stable, unlike many cable driven mechanisms. The lack of interference with cables could extend their workspace and simplify their practical implementation.

This paper introduces a spatial, three-degree-of-freedom (3-DoF) mechanism based on a known tensegrity architecture. The element selection and actuation scheme of the mechanism are discussed and geometric proof is shown that the mechanism can be made to move in pure translational motion. Translational motion is useful in several applications, including industrial "pick and place" operations where a gripper on the end of the manipulator allows for the rapid positioning and assembly of parts. The inverse and direct kinematics of the mechanism are solved and used to determine the boundaries of the workspace attainable by the mechanism's end-effector.

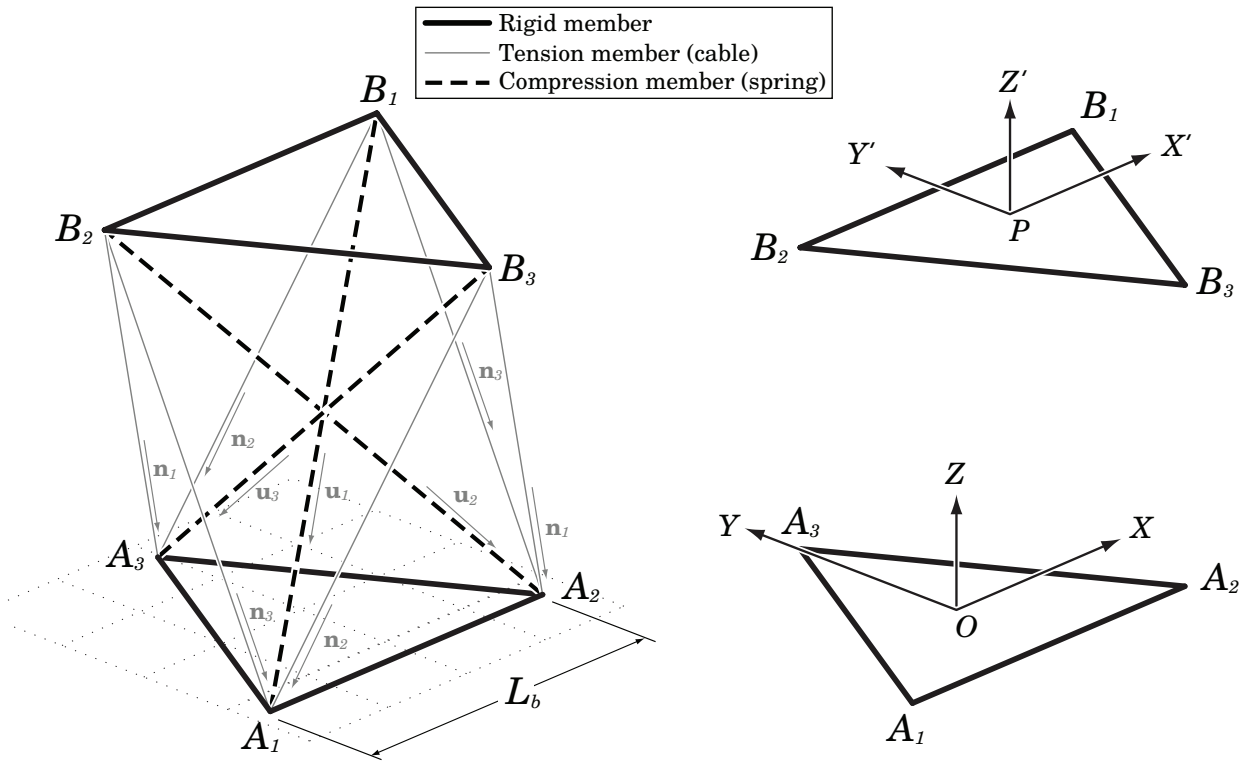

Figure 1: Schematic of the 3-DoF spatial mechanism.

2 DESCRIPTION OF MECHANISM ARCHITECTURE

The mechanism discussed in this paper is based on the reinforced tensegrity octahedron (or simplex) architecture proposed by Knight [2]. As shown in Fig. 1, it is comprised of three compressive members, joining nodes A_1B_1, A_2B_2 and A_3B_3, and six tensile members, joining nodes A_1B_2, A_1B_3, A_2B_1, A_2B_3, A_3B_1 and A_3B_2. The nodes also form two congruent equilateral triangles: $A_1A_2A_3$, which is fixed to ground, and $B_1B_2B_3$, which acts as the mechanism's end-effector. Both triangles have a side length of L_b and the end-effector triangle may be considered a solid plate, allowing for the attachment of tools or grasping devices.

The fixed reference frame, XYZ, used to describe the motion of the mechanism is shown in Fig. 1. It is located at point O, the centroid of the base triangle, with the X axis aligned with the line between nodes A_1 and A_2, the Y axis passing through node A_3, and the Z axis normal to the plane formed by nodes $A_1A_2A_3$. Within this reference frame, the A_i nodes, $(i = 1, 2, 3)$, are located by the following vectors:

$$\mathbf{a}_1 = L_b \begin{bmatrix} \frac{-1}{2} \\ \frac{-\sqrt{3}}{6} \\ 0 \end{bmatrix} \qquad \mathbf{a}_2 = L_b \begin{bmatrix} \frac{1}{2} \\ \frac{-\sqrt{3}}{6} \\ 0 \end{bmatrix} \qquad \mathbf{a}_3 = L_b \begin{bmatrix} 0 \\ \frac{\sqrt{3}}{3} \\ 0 \end{bmatrix} \tag{1}$$

The centroid of the mechanism's end-effector, P, is located in the XYZ frame by the position vector $\mathbf{p} = [x, y, z]^\mathsf{T}$. A second, mobile reference frame, $X'Y'Z'$, is attached to the end-effector

at this point and is initially aligned with XYZ. Within the $X'Y'Z'$ frame, the three nodes of the end-effector, B_i, are located by the following vectors:

$$\mathbf{b}_1 = L_b \begin{bmatrix} \frac{1}{2} \\ \frac{\sqrt{3}}{6} \\ 0 \end{bmatrix} \qquad \mathbf{b}_2 = L_b \begin{bmatrix} \frac{-1}{2} \\ \frac{\sqrt{3}}{6} \\ 0 \end{bmatrix} \qquad \mathbf{b}_3 = L_b \begin{bmatrix} 0 \\ \frac{-\sqrt{3}}{3} \\ 0 \end{bmatrix} \tag{2}$$

This mechanism differs from existing tensegrity mechanisms based on the reinforced octahedron [6, 11] in the way it is prestressed and actuated. It utilizes three compression springs to maintain prestress in each of its components, while six cables of variable length supply tension to maintain static equilibrium. The compressive members are attached via universal joints to the base, at A_i, and spherical joints to the end-effector, at B_i. The flexibility of the cables used as tensile members eliminate the need for additional, coincident spherical or universal joints. Instead they can be routed through each joint, similar to the method described by Schenk [12], and actuated by a motorized winch below the base. This particular architecture is beneficial for its ability to automatically find tensegrity configurations, since when given a set of cable lengths it will naturally deform to a stable configuration to minimize its potential energy.

One obstacle with the physical implementation of the mechanism is the interference of the compressive elements at their respective midpoints (as shown in Fig. 1). This can be shown to exist in all of the equilibrium configurations of the mechanism. To overcome this issue, each compression element is replaced with a non-interfering spring design, shown in Fig. 2. The design incorporates two rigid links of length $L_o/2$ that are connected to each other via a revolute joint. A torsion spring is located at the revolute joint and applies a torque, τ_i, based on the angle, $2\theta_i$, between the links. The "virtual" spring will thus have a compressive force, F_i, along its effective length L_i. Each set of links is attached to the base using a universal joint and to the end-effector with a spherical joint. The second axis of the universal joint is parallel to the revolute joint of the links while the first is orthogonal to both the second axis and the vector $\mathbf{a}_i$. This constrains each set of links to act within a plane whose normal is the second universal joint axis.

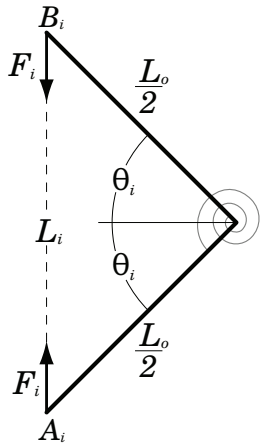

Figure 2: Illustration of the proposed virtual compression spring design.

The half angle, θ_i, between the two links in each spring is defined as

$$\theta_i = \arcsin\left(\frac{L_i}{L_o}\right) \tag{3}$$

Assuming that the torsion spring behaves linearly and is at rest when $\theta_i = \theta_o = \pi/2$ (*i.e.*, when it is fully extended), it applies a torque, τ_i, equal to

$$\tau_i = \kappa(2\theta_i - \pi) \tag{4}$$

where κ is the torsion spring constant, assumed to be the same for all three springs. By taking a moment balance about each revolute joint, the force that each virtual spring exerts is found to be

$$F_i = \frac{2\kappa\left[2\arcsin\left(\frac{L_i}{L_o}\right) - \pi\right]}{L_o\sqrt{1 - \left(\frac{L_i}{L_o}\right)^2}} \tag{5}$$

which will be a compressive force applied parallel to the virtual spring length. All of the mechanism's elements will now be considered in compression if their internal force is negative and in tension when their force is positive.

With this design, the length L_o can be chosen to avoid interference between the links of the virtual compression springs and cables. This is found to be possible based on a brief inspection and full analysis of the interference will follow in future work. Additionally, it theoretically allows the virtual spring to have the full range of $0 < L_i < L_o$, potentially maximizing the size of the mechanism's workspace.

The development of the mechanism's architecture is based on the desire to reduce the mass of moving parts, to simplify actuation, and to generate pure translational motion of the end-effector. To this effect, one may observe the occurrence of the three parallelograms, $A_1A_2B_1B_2$, $A_2A_3B_2B_3$, and $A_3A_1B_3B_1$, formed by the mechanism's elements and demonstrated in Fig. 3. The arrangement of these parallelograms presents an opportunity to ensure that the movement of the end-effector triangle is translational only. If the cables remain taut and are actuated in appropriate pairs, as shown in Table 1, the end-effector will remain parallel to the ground. Actuation of the mechanism could be achieved by using a single motorized winch to drive each pair of cables (total of three winches), further simplifying the mechanism's architecture. The input variables of the mechanism are thus the cable lengths $\boldsymbol{\psi} = [\rho_1, \rho_2, \rho_3]^\mathsf{T}$ and the output variables are the components of the position vector $\mathbf{p} = [x, y, z]^\mathsf{T}$.

Table 1: Actuated pairs of cables.

Length	Cable Pair
ρ_1	A_2B_3, A_3B_2
ρ_2	A_1B_3, A_3B_1
ρ_3	A_1B_2, A_2B_1

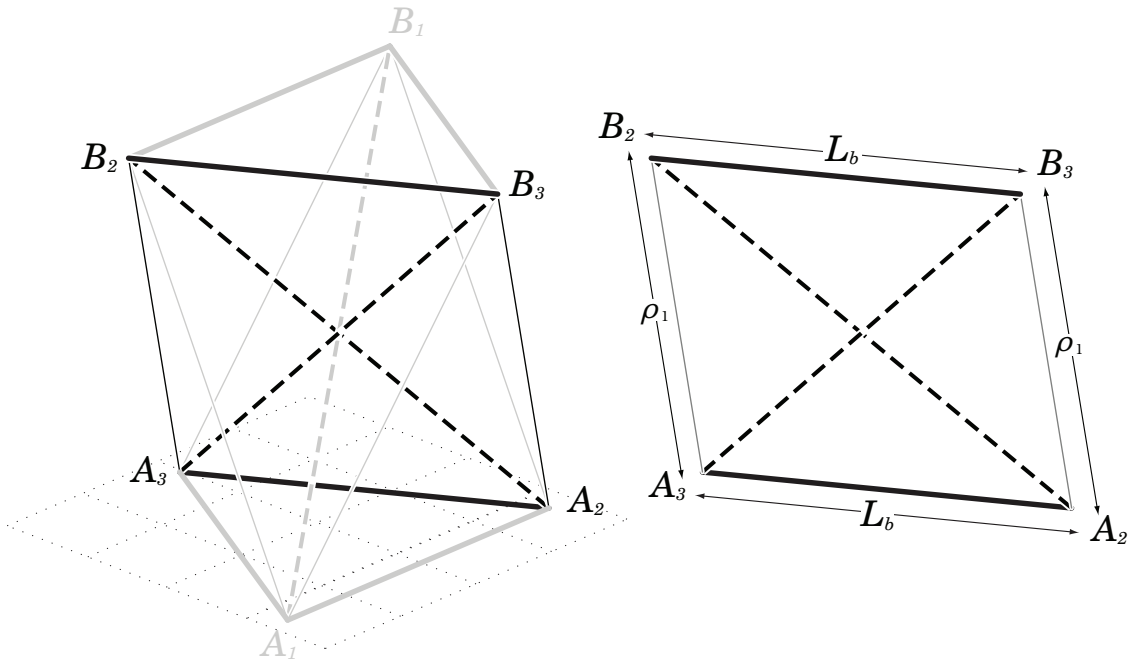

Figure 3: Location of the parallelogram $A_2B_3B_2A_3$ with respect to the rest of the mechanism.

3 SOLUTIONS TO THE DIRECT AND INVERSE KINEMATIC PROBLEMS

For the purpose of this paper, the direct and inverse kinematic problems are solved for the case in which the cables are assumed inextensible and taut and the base and end-effector triangles are perfectly rigid.

3.1 Direct Kinematic Problem

The direct kinematic problem (DKP) is the task of determining the output variables, $\mathbf{p}$, of the mechanism when supplied with the input variables, $\boldsymbol{\psi}$. Since the lengths of all six cables are known and assumed to be taut, the location of the end-effector can be found through a vector loop closure method. The length of each cable can be determined through one of two separate, equivalent vector loops:

$$\rho_1^2 = (\mathbf{p} + \mathbf{b}_3 - \mathbf{a}_2)^\mathsf{T}(\mathbf{p} + \mathbf{b}_3 - \mathbf{a}_2) = (\mathbf{p} + \mathbf{b}_2 - \mathbf{a}_3)^\mathsf{T}(\mathbf{p} + \mathbf{b}_2 - \mathbf{a}_3) \tag{6}$$

$$\rho_2^2 = (\mathbf{p} + \mathbf{b}_1 - \mathbf{a}_3)^\mathsf{T}(\mathbf{p} + \mathbf{b}_1 - \mathbf{a}_3) = (\mathbf{p} + \mathbf{b}_3 - \mathbf{a}_1)^\mathsf{T}(\mathbf{p} + \mathbf{b}_3 - \mathbf{a}_1) \tag{7}$$

$$\rho_3^2 = (\mathbf{p} + \mathbf{b}_2 - \mathbf{a}_1)^\mathsf{T}(\mathbf{p} + \mathbf{b}_2 - \mathbf{a}_1) = (\mathbf{p} + \mathbf{b}_1 - \mathbf{a}_2)^\mathsf{T}(\mathbf{p} + \mathbf{b}_1 - \mathbf{a}_2) \tag{8}$$

where the orientation of the end-effector remains aligned with the base due to the existence of the parallelograms developed in Section 2. It can be recognized that, when the end-effector reference frame ($X'Y'Z'$) is aligned with the base's (XYZ), $\mathbf{b}_i = -\mathbf{a}_i$ and the sum of any two of the $\mathbf{a}_i$ vectors is equal to the negative of the third. Then, using either set of vector loops presented in

Eqs. (6) through (8), the actuator lengths are found to be equivalent to

$$\rho_i^2 = (\mathbf{p} + \mathbf{a}_i)^\mathsf{T}(\mathbf{p} + \mathbf{a}_i) \tag{9}$$

Expanding these equations leads to a general expression for the length of cable i in terms of the unknown position vector $\mathbf{p}$ and the known vectors $\mathbf{a}_i$ as follows:

$$\rho_i^2 = \mathbf{p}^\mathsf{T}\mathbf{p} + 2\mathbf{p}^\mathsf{T}\mathbf{a}_i + \mathbf{a}_i{}^\mathsf{T}\mathbf{a}_i = x^2 + y^2 + z^2 + 2xa_{i_x} + 2ya_{i_y} + a_{i_x}^2 + a_{i_y}^2 \tag{10}$$

Solving Eq. (10) for x, y, and z gives

$$x = \frac{(\rho_2^2 - \rho_1^2)}{2L_b} \tag{11}$$

$$y = \frac{(2\rho_3^2 - \rho_2^2 - \rho_1^2)}{2\sqrt{3}L_b} \tag{12}$$

$$z = \pm\frac{\sqrt{-\rho_1^4 - \rho_2^4 - \rho_3^4 + \rho_1^2\rho_2^2 + \rho_1^2\rho_3^2 + \rho_2^2\rho_3^2 + L_b^2(\rho_1^2 + \rho_2^2 + \rho_3^2 - L_b^2)}}{\sqrt{3}L_b} \tag{13}$$

This shows that there are two solutions to the DKP for every input $\boldsymbol{\psi}$, one of them corresponds to a configuration above the XY plane and the other to the same configuration below the XY plane. Only one of these configurations is possible for the mechanism to achieve without colliding with its base, therefore the solution with a negative z value is ignored. Thus the solution to the DKP is a one-to-one mapping between the actuator space and Cartesian space.

3.2 Inverse Kinematic Problem

The inverse kinematic problem (IKP) is the task of determining the actuator variables, $\boldsymbol{\psi}$, required to achieve a given position of the mechanism's end-effector, $\mathbf{p}$. Similar to other parallel mechanisms, the process of solving the IKP for this mechanism is relatively straightforward.

When given the position of the end-effector platform, points B_i are known and the same vector loops used in the DKP can be used to determine the lengths of each cable pair. Taking the square root of Eq. (9) gives

$$\rho_i = \sqrt{(\mathbf{p} + \mathbf{a}_i)^\mathsf{T}(\mathbf{p} + \mathbf{a}_i)} \tag{14}$$

which is the solution to the IKP.

4 Determination of Cartesian Workspace Boundaries

The Cartesian workspace of the mechanism is defined as the three-dimensional volume of space containing all values of $\mathbf{p}$ that can be attained by the mechanism in stable tensegrity configurations. The workspace boundaries are based on two sets of constraints: kinematic constraints such as the minimum and maximum lengths of the springs, and the constraint requiring that the mechanism always be in static equilibrium with the cables in tension. Again, the workspace is based on the special conditions of inextensible cables and a perfectly rigid base and end-effector. The methods presented also consider only internal forces, assuming gravity and external forces to be zero.

4.1 Kinematic Constraints

The first boundary of the workspace is simply the XY plane, since the position of the end-effector cannot pass through this plane or the mechanism will collide with itself. In reality, physical limitations, such as those imposed by the mechanism's joints, would also prevent this from occurring.

The other boundaries are dependent on the minimum and maximum attainable lengths of the mechanism's actuators and compression springs. Since practically any length of cable can be wound onto the mechanism's actuators (motorized winches), the actuator lengths are left unconstrained. However, the compression springs will have physical restrictions on their effective lengths, L_i. The effective length is found to be

$$(\mathbf{p} + \mathbf{b}_i - \mathbf{a}_i)^\mathsf{T}(\mathbf{p} + \mathbf{b}_i - \mathbf{a}_i) = L_i^2 \tag{15}$$

Letting the minimum and maximum length of each compression spring be L_{min} and L_{max}, respectively, and recognizing that when the end-effector has no rotation $\mathbf{b}_i = -\mathbf{a}_i$, Eq. (15) can be rewritten as the following constraints:

$$(\mathbf{p} - 2\mathbf{a}_i)^\mathsf{T}(\mathbf{p} - 2\mathbf{a}_i) \geq L_{min}^2 \tag{16}$$

$$(\mathbf{p} - 2\mathbf{a}_i)^\mathsf{T}(\mathbf{p} - 2\mathbf{a}_i) \leq L_{max}^2 \tag{17}$$

which are the equations of spheres centred at $2\mathbf{a}_i$ with a radius of either L_{min} or L_{max}. The workspace volume is then the volumes of the three smaller spheres (of radius L_{min}) subtracted from the intersection of the three larger spheres (of radius L_{max}). Based solely on these kinematic constraints, an example of the Cartesian workspace is shown in Fig. 4, using the range of $0 \leq L_i \leq L_o$ and the arbitrary value of $L_{max} = L_o = 3L_b$. The torsion spring within the virtual compression member design is assumed to be capable of this full range.

4.2 Static Constraints

The Cartesian workspace is further constrained based on the requirements that the mechanism always be in a state of self stress and the cables remain in tension. To determine whether a given configuration satisfies the equilibrium and tension requirements, the wrench, $\mathbf{w}$, of the end-effector is found as

$$\mathbf{w} = \mathbf{W}_f\mathbf{f} + \mathbf{W}_t\mathbf{t} = \mathbf{0} \tag{18}$$

where

$$\mathbf{W}_f = \begin{bmatrix} \mathbf{u}_1 & \mathbf{u}_2 & \mathbf{u}_3 \\ \mathbf{b}_1 \times \mathbf{u}_1 & \mathbf{b}_2 \times \mathbf{u}_2 & \mathbf{b}_3 \times \mathbf{u}_3 \end{bmatrix} \tag{19}$$

and

$$\mathbf{W}_t = \begin{bmatrix} \mathbf{n}_1 & \mathbf{n}_2 & \mathbf{n}_3 & \mathbf{n}_1 & \mathbf{n}_2 & \mathbf{n}_3 \\ \mathbf{b}_3 \times \mathbf{n}_1 & \mathbf{b}_3 \times \mathbf{n}_2 & \mathbf{b}_2 \times \mathbf{n}_3 & \mathbf{b}_2 \times \mathbf{n}_1 & \mathbf{b}_1 \times \mathbf{n}_2 & \mathbf{b}_1 \times \mathbf{n}_3 \end{bmatrix} \tag{20}$$

are the wrench matrices that relate the magnitude of the forces within each element to the force and moment they apply on the end-effector. The unit vectors $\mathbf{n}_i$ and $\mathbf{u}_i$ are aligned with the corresponding mechanism's elements, as shown in Fig. 1. Furthermore, the vectors $\mathbf{f}$ and $\mathbf{t}$ are

$$\mathbf{f} = [F_1, F_2, F_3]^\mathsf{T} \tag{21}$$

$$\mathbf{t} = [t_1, t_2, t_3, t_4, t_5, t_6]^\mathsf{T} \tag{22}$$

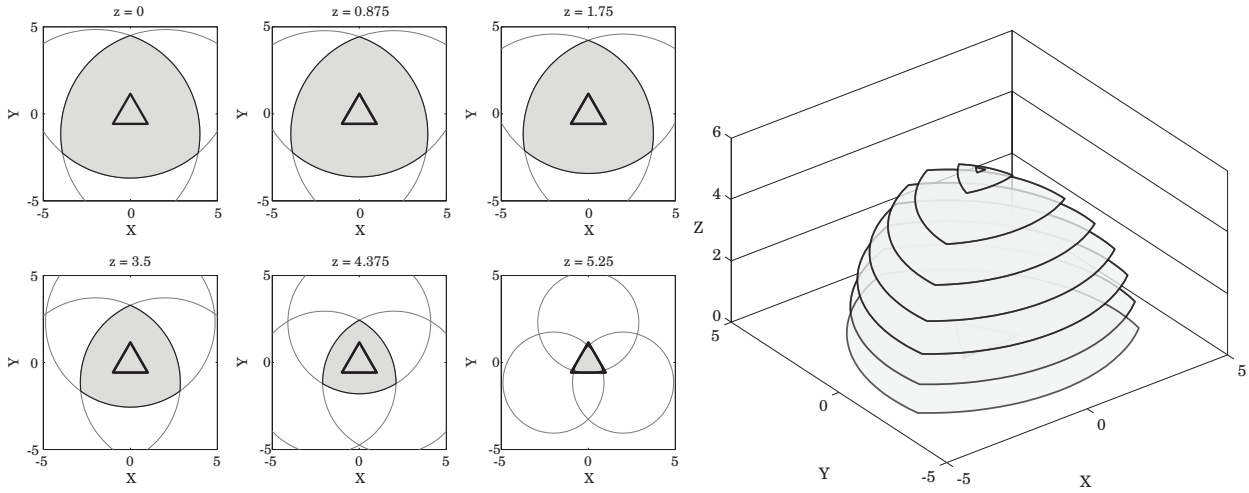

Figure 4: Horizontal slices of the Cartesian workspace at various heights (z) based only on kinematic constraints with $L_b = 2$, $L_{min} = 0$ and $L_{max} = L_o = 3L_b$. The base triangle $A_1A_2A_3$ is shown for size reference.

with F_i being the force within the ith spring (as determined by Eq. (5)) and t_j being the corresponding force of the jth cable, ($j = 1, 2, \ldots, 6$). In the definitions of F_i and t_j, compression is considered to be a negative force, tension positive.

The boundaries of the workspace correspond to the loss of tension in one or more cables. To find where tension is lost Eq. (18) is solved by using the inverse of the $\mathbf{W}_t$ matrix:

$$\mathbf{t} = -\mathbf{W}_t^{-1}\mathbf{W}_f\mathbf{f} \tag{23}$$

This method is valid so long as $\mathbf{W}_t$ is invertible. The determinant of $\mathbf{W}_t$ is found to be

$$\det(\mathbf{W}_t) = \frac{-3\sqrt{3}}{4}\left(\frac{z^3 L_b^6}{\rho_1^2\rho_2^2\rho_3^2}\right) \tag{24}$$

which shows that $\mathbf{W}_t$ would cease to be invertible when $z = 0$. However, since a configuration of the mechanism with $z = 0$ would cause its elements to collide with its base or each other, the singularity condition will be avoided in practice. Additionally, it can be observed from Eq. (9) that the length of the ith actuator, ρ_i, will only equal zero when the mechanism's end-effector is in a position such that $\mathbf{p} = -\mathbf{a}_i$. The vectors $\mathbf{a}_i$ have no Z component and thus these configurations will occur at the same time as the singularity identified above.

Solving Eq. (23) for t_j in terms of the spring forces F_i yields

$$t_1 = t_4 = \frac{\rho_1}{2}\left(+\frac{F_1}{L_1} - \frac{F_2}{L_2} - \frac{F_3}{L_3}\right) \tag{25}$$

$$t_2 = t_5 = \frac{\rho_2}{2}\left(-\frac{F_1}{L_1} + \frac{F_2}{L_2} - \frac{F_3}{L_3}\right) \tag{26}$$

$$t_3 = t_6 = \frac{\rho_3}{2}\left(-\frac{F_1}{L_1} - \frac{F_2}{L_2} + \frac{F_3}{L_3}\right) \tag{27}$$

where ρ_i and L_i are functions of $\mathbf{p}$ as shown in Eqs. (14) and (15), respectively. The values within the brackets can be further simplified through the use of force densities (also referred to as tension coefficients, *e.g.*, [13]) defined as $\hat{f}_i = F_i/L_i$. For the mechanism's cables to be in tension, Eqs. (25) through (27) must remain greater than zero and thus the following three conditions are arrived at:

$$\left(+\hat{f}_1 - \hat{f}_2 - \hat{f}_3\right) > 0 \tag{28}$$

$$\left(-\hat{f}_1 + \hat{f}_2 - \hat{f}_3\right) > 0 \tag{29}$$

$$\left(-\hat{f}_1 - \hat{f}_2 + \hat{f}_3\right) > 0 \tag{30}$$

These equations describe the boundaries of three volumes of space. The intersection of these boundaries contain all equilibrium configurations of the mechanism where tension is maintained in all cables.

The workspace may be visualized for the spring design introduced in Section 2 by substituting values of F_i, based on Eq. (5), into Eqs. (25) through (27). Again using the arbitrary maximum

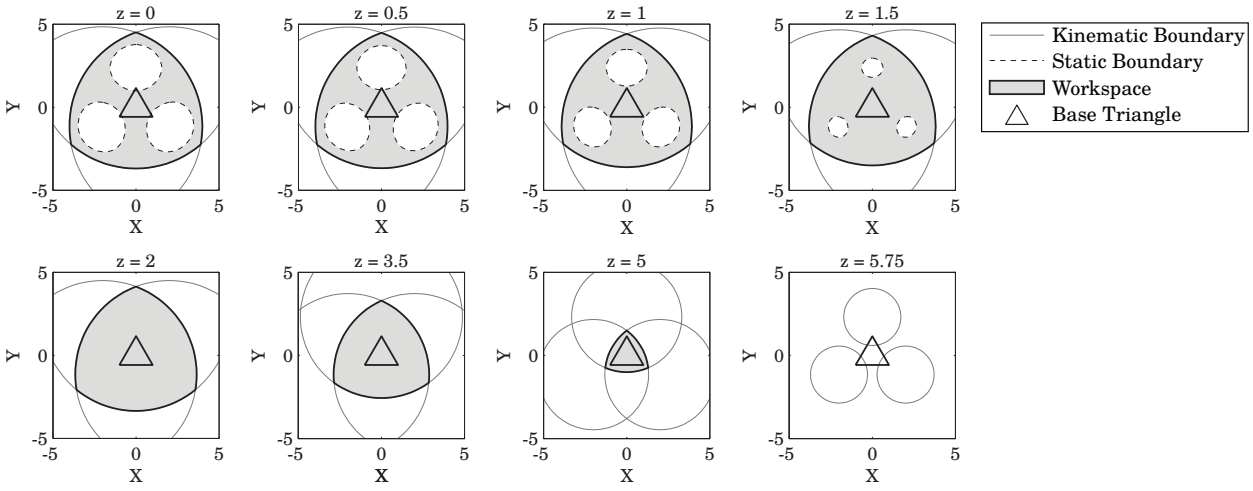

Figure 5: Horizontal slices of the Cartesian workspace at various heights (z) based on both static and kinematic constraints with $L_b = 2$ and $L_o = 3L_b$.

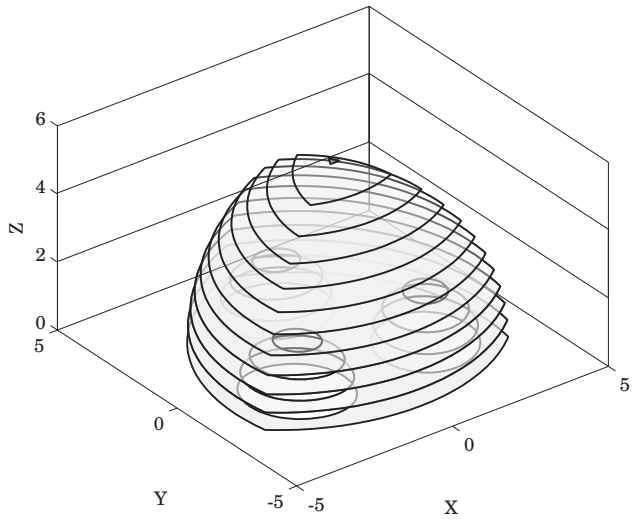

Figure 6: Cartesian workspace based on both static and kinematic constraints with $L_b = 2$ and $L_o = 3L_b$.

effective spring length of $L_o = 3L_b$, the boundaries of this static workspace are shown in Fig. 5 and Fig. 6. The outer boundaries correspond to one or more of the springs becoming fully extended and no longer applying any compressive force. Therefore, these are the same as the kinematic boundaries previously found when $L_i = L_{max}$. The inner boundaries are based on the static constraints and are independent of the spring stiffness used.

5 CONCLUSIONS

This paper presented a novel spatial mechanism based on the principles of tensegrity and actuated by cables. Translational motion of the mechanism's end-effector through Cartesian space was achieved using strategic actuation of the cables. Simple analytic solutions to the direct and inverse kinematic problems were produced, based on the assumption that the mechanism remained in a state of self-stress with cables in tension. Testing the assumption revealed the boundaries to the attainable workspace of the mechanism and thus to the space within which the analytical solutions are valid. These boundaries were clearly defined and shown to be dependent on the length of the spring links and independent of their stiffness.

The workspace presented did not consider gravitational or external forces being applied to the mechanism. However, the author believes that if the mechanism were oriented favourably with gravity, the mass of the mechanism and any payload will add to the tension within the mechanism and increase its workspace. Pick and place operations, where the mechanism is located above its workspace and gravity acts in a downward direction, are a potential application that would benefit from this larger workspace. Additionally, the workspace theoretically includes the XY plane. Therefore the mechanism is capable of being actuated into a flattened configuration and can be deployed from a very small volume. Further work by the author is planned to investigate the effects of external loads in greater detail as well as what constraints, if any, are placed on the workspace due to interference between elements.

REFERENCES

[1] B. Fuller. Tensile-integrity structures. United States Patent No 3,063,521, November 1962.

[2] B. Knight. *Deployable Antenna Kinematics Using Tensegrity Structure Design*. PhD thesis, University of Florida, 2000.

[3] C. Sultan, M. Corless, and R. Skelton. Tensegrity flight simulator. *Journal of Guidance, Control and Dynamics*, 23(6):1055–1064, 2000.

[4] C. Paul, J. W. Roberts, H. Lipson, and F. V. Cueva. Gait production in a tensegrity based robot. In *Advanced Robotics, ICAR '05*, pages 216–222, 2005.

[5] J. B. Aldrich and R Skelton. Backlash-free motion control of robotic manipulators driven by tensegrity motor networks. In *45th IEEE Conference on Decision and Control*, pages 2300–2306, San Diego, CA, USA, December 2006.

[6] M. Arsenault and C. Gosselin. Dynamic simulation of a spatial 3-DOF tensegrity mechanism. *Transactions of the Canadian Society for Mechanical Engineering*, 29(4):491–506, 2005.

[7] S. Chen and M. Arsenault. Workspace computation and analysis of a planar 2-DOF translational tensegrity mechanism. In *ASME IDETC/CIE 2010*, Montreal, Quebec, Canada, August 2010.

[8] C. Sultan and R. Skelton. Deployment of tensegrity structures. *International Journal of Solids and Structures*, 40:4637–4657, 2003.

[9] J. Duffy, J. Rooney, B. Knight, and C. D. Crane. A review of a family of self-deploying tensegrity structures with elastic ties. *Shock and Vibration Digest*, 32(2):100–106, 2000.

[10] J. Mirats Tur. On the movement of tensegrity structures. *International Journal of Space Structures*, 25(1):1–14, 2010.

[11] M. Arsenault and C. Gosselin. Kinematic, static, and dynamic analysis of a spatial three-degree-of-freedom tensegrity mechanism. *Journal of Mechanical Design*, 128(5):1061–1069, 2006.

[12] M. Schenk. Statically balanced tensegrity mechanisms. Master's thesis, Delft University of Technology, 2006.

[13] S. Guest. The stiffness of prestressed frameworks: A unifying approach. *International Journal of Solids and Structures*, 43:842–854, 2006.